HHS Public Access

Author manuscript

Radiology. Author manuscript; available in PMC 2015 March 24.

Published in final edited form as:

Radiology. 2015 March ; 274(3): 790–799. doi:10.1148/radiol.14140568.

Vascular Endothelial Growth Factor Receptor Type 2–targeted Contrast-enhanced US of Pancreatic Cancer Neovasculature in a Genetically Engineered Mouse Model: Potential for Earlier Detection

Marybeth A. Pysz, PhD[2], **Steven B. Machtaler, PhD**, **E. Scott Seeley, MD, PhD**, **John J. Lee, MD, PhD**, **Teresa A. Brentnall, MD**, **Jarrett Rosenberg, PhD**, **François Tranquart, MD, PhD**, and **Jürgen K. Willmann, MD**

Department of Radiology, Molecular Imaging Program at Stanford (MIPS), Stanford School of Medicine, Stanford University, 300 Pasteur Dr, Room H1307, Stanford, CA 94305 (M.A.P., S.B.M., J.R., J.K.W.); Department of Pathology, University of California at San Francisco, San Francisco, Calif (E.S.S.); Department of Developmental Biology, Institute for Stem Cell Biology and Regenerative Medicine, Howard Hughes Medical Institute, Stanford School of Medicine, Stanford University, Stanford, Calif (J.J.L.); Department of Medicine, University of Washington, Seattle, Wash (T.A.B.); and Bracco Suisse SA, Geneva, Switzerland (F.T.)

Abstract

Purpose—To test ultrasonographic (US) imaging with vascular endothelial growth factor receptor type 2 (VEGFR2)-targeted microbubble contrast material for the detection of pancreatic ductal adenocarcinoma (PDAC) in a transgenic mouse model of pancreatic cancer development.

Materials and Methods—Experiments involving animals were approved by the Institutional Administrative Panel on Laboratory Animal Care at Stanford University. Transgenic mice (n = 44; Pdx1-Cre, $KRas^{G12D}$, $Ink4a^{-/-}$) that spontaneously develop PDAC starting at 4 weeks of age were imaged by using a dedicated small-animal US system after intravenous injection of 5×10^7 clinical-grade VEGFR2-targeted microbubble contrast material. The pancreata in wild-type (WT)

Address correspondence to J.K.W. (willmann@stanford.edu).

[2]**Current address:** Stem CentRx, South San Francisco, Calif.

Author contributions:

Guarantors of integrity of entire study, M.A.P., J.K.W.; study concepts/study design or data acquisition or data analysis/interpretation, all authors; manuscript drafting or manuscript revision for important intellectual content, all authors; approval of final version of submitted manuscript, all authors; agrees to ensure any questions related to the work are appropriately resolved, all authors; literature research, M.A.P., S.B.M., T.A.B., J.K.W.; experimental studies, M.A.P., S.B.M., E.S.S., J.J.L., J.K.W.; statistical analysis, S.B.M., J.R., J.K.W.; and manuscript editing, M.A.P., S.B.M., E.S.S., J.J.L., T.A.B., J.K.W.

Disclosures of Conflicts of Interest: M.A.P. Activities related to the present article: Bracco Suisse provided the microbubble contrast reagents used in this study. Activities not related to the present article: disclosed no relevant relationships. Other relationships: disclosed no relevant relationships. **S.B.M.** disclosed no relevant relationships. **E.S.S.** disclosed no relevant relationships. **J.J.L.** disclosed no relevant relationships. **T.A.B.** disclosed no relevant relationships. **J.R.** disclosed no relevant relationships. **F.T.** Activities related to the present article: Bracco Suisse provided the microbubble contrast reagents used in this study. Activities not related to the present article: author is an employee of Bracco Suisse. Other relationships: disclosed no relevant relationships. **J.K.W.** Activities related to the present article: disclosed no relevant relationships. Activities not related to the present article: author received payment from Bracco for consulting. Other relationships: disclosed no relevant relationships.

Online supplemental material is available for this article.

mice (n = 64) were scanned as controls. Pancreatic tissue was analyzed ex vivo by means of histologic examination (with hematoxylin-eosin staining) and immunostaining of vascular endothelial cell marker CD31 and VEGFR2. The Wilcoxon rank sum test and linear mixed-effects model were used for statistical analysis.

Results—VEGFR2-targeted US of PDAC showed significantly higher signal intensities (26.8-fold higher; mean intensity ± standard deviation, 6.7 linear arbitrary units [lau] ± 8.5; $P < .001$) in transgenic mice compared with normal, control pancreata of WT mice (mean intensity, 0.25 lau ± 0.25). The highest VEGFR2-targeted US signal intensities were observed in smaller tumors, less than 3 mm in diameter (30.8-fold higher than control tissue with mean intensity of 7.7 lau ± 9.3 [$P < .001$]; and 1.7-fold higher than lesions larger than 3 mm in diameter with mean intensity of 4.6 lau ± 5.8 [$P < .024$]). Ex vivo quantitative VEGFR2 immunofluorescence demonstrated that VEGFR2 expression was significantly higher in pancreatic tumors ($P < .001$; mean fluorescent intensity, 499.4 arbitrary units [au] ± 179.1) compared with normal pancreas (mean fluorescent intensity, 232.9 au ± 83.7).

Conclusion—US with clinical-grade VEGFR2-targeted microbubbles allows detection of small foci of PDAC in transgenic mice.

Pancreatic ductal adenocarcinoma (PDAC) is the fourth leading cause of cancer-related death, with a mean 5-year survival rate of 6%. In 2013, 45 220 new cases of PDAC were diagnosed in the United States, with an estimated 38 460 patients succumbing to the disease (1). More than 80% of patients with new diagnoses have nonresectable, advanced disease (median survival, 4–6 months [2]), and more than 65% of surgical candidates will develop disease recurrence within 2 years after surgery (3). Several studies have shown that long-term survival after PDAC resection increases with small tumor size, with a 5-year survival time of more than 75% when the primary tumor can be diagnosed with a diameter of less than 1 cm (2,4–6). Therefore, developing an early detection approach for PDAC detection holds great promise for improving the poor prognosis of patients with this devastating disease.

A multimodality screening approach of endoscopic ultrasonography (US) and magnetic resonance (MR) cholangiopancreatography has been proposed as a possible approach to screen for PDAC in high-risk patients (7,8). However, MR cholangiopancreatography has limited sensitivity in detecting small pancreatic lesions, and its substantial cost is disadvantageous for screening programs (9–11). Although endoscopic US has shown the highest sensitivity in detecting small PDAC lesions compared with other imaging modalities, it is operator dependent. Detection of PDAC with endoscopic US relies on the identification of several morphologic imaging criteria of precursor or early PDAC at B-mode imaging, including parenchymal heterogeneity, echogenic foci, and hypoechoic nodules, which are subtle. It has been demonstrated that the interobserver agreement of 17 expert endosonographers who interpreted endoscopic US images in high-risk patients was only fair to poor and did not improve, even with consensus interpretations (12). Other studies have shown enhanced detection sensitivity of endoscopic US when paired with nontargeted US contrast agents (microbubbles), which can highlight irregularities in vascular networks and vascular flow patterns (13–15). Contrast material–enhanced transabdominal US of the pancreas is also currently being explored, which may be a

noninvasive and cost-effective alternative to endoscopic US in patients with appropriate acoustic window to visualize the pancreas (16–18).

Advances in Knowledge

- Small pancreatic ductal adenocarcinoma (PDAC) lesions in the Pdx1-Cre$^{tg/+}$, KRas$^{LSL\ G12D/+}$, Gli-1$^{LacZ/+}$, Ink4a/Arf$^{-/-}$ transgenic mouse model express vascular endothelial growth factor receptor type 2 (VEGFR2) within the neovasculature that can readily be detected by using US with a clinical-grade VEGFR2-targeted microbubble contrast agent.
- Mean US signal of VEGFR2-targeted contrast enhancement is 26.8-fold higher in PDAC lesions compared with normal pancreatic tissue.
- PDAC lesions smaller than 3 mm have higher mean VEGFR2-targeted US signal compared with PDAC lesions larger than 3 mm in diameter.

The diagnostic accuracy of US in detecting PDAC could be further improved by using a microbubble contrast material engineered to bind proteins differentially expressed in the neovasculature of cancer. Neoangiogenesis, the process of new vascular growth from existing vascular networks or circulating endothelial stem cells, plays a key role in tumor growth beyond 0.2–2 mm in diameter (19–21). Molecular imaging of neovascular markers, such as vascular endothelial growth factor receptor type 2 (VEGFR2), which plays an important role in tumor neoangiogenesis of many cancers, including PDAC (22–26), may be an elegant approach for detecting PDAC at an early and still treatable stage, just after the angiogenic switch has occurred during tumor progression (27). Furthermore, it has been shown (26) that VEGFR2 expression levels in human PDAC cells and PDAC-associated vascular endothelial cells are increased when compared with those in normal pancreas and chronic pancreatitis, suggesting that VEGFR2 may be an appropriate biomarker for imaging PDAC in patients.

Implication for Patient Care

- The results reported in this study lay the foundation for the potential use of US with molecularly targeted contrast agents for the detection of PDAC in high-risk patients.

The purpose of this study was to test a US strategy with VEGFR2-targeted microbubble contrast agent for pancreatic cancer detection in a transgenic mouse model of PDAC development.

Materials and Methods

Bracco Suisse provided the clinically translatable contrast agent used in this study. Authors who were not employees of Bracco Suisse (M.A.P., S.B.M., E.S.S., J.J.L., T.A.B., J.R., J.K.W.) had control over inclusion of any data and information that might have presented a conflict of interest for authors who were employees of Bracco Suisse (F.T.).

Transgenic Mouse Model of PDAC

All experiments involving animals were approved by the Institutional Administrative Panel on Laboratory Care at Stanford University. The transgenic PDAC mouse model of Pdx1-$Cre^{tg/+}$, $KRas^{LSL\ G12D/+}$, $Gli1^{LacZ/+}$, Ink4a/$Arf^{-/-}$, similar to that described by Aguirre et al (28), was used (denoted as PDAC mice). These mice spontaneously develop foci of PDAC within 4–7 weeks of age and closely recapitulate human disease progression and morphology (28). Age-matched littermates without the $KRas^{G12D}$ mutation (genotyped negative) were used as normal control wild type (WT) mice (denoted as WT mice). Mice were bred and genotyped (Mouse Genotype, Escondido, Calif) by M.A.P. (with 4 years of experience), E.S.S. (with 10 years of experience), and J.J.L. (with 10 years of experience).

US with VEGFR2-targeted Microbubbles

Forty-four PDAC mice with a total of 90 tumors and 64 WT mice were scanned with US. The diameter of tumors in the body and/or tail ($n = 75$) and head ($n = 15$) of the pancreas ranged between 0.7 and 7 mm (0–2 mm, $n = 40$; 2–3 mm, $n = 22$; 3–4 mm, $n = 10$; 4–5 mm, $n = 11$; and >5 mm, $n = 7$) as measured with US by using electronic calipers.

Beginning at 3 weeks of age, the pancreata of all mice were imaged twice weekly (by M.A.P.) in the transverse and sagittal planes by using a dedicated small-animal US system (Vevo2100; VisualSonics, Toronto, Ontario, Canada). The detailed protocol is described in Appendix E1 (online). Briefly, 40-MHz B-mode imaging was used to identify lesions suspicious for cancer (hypoechoic foci), and once a lesion was identified, the 40-MHz transducer was fixed into position on the imaging platform and switched with the 21-MHz transducer for nonlinear contrast-enhanced imaging (Fig 1; see Appendix E1 [online]). Contrast-enhanced perfusion and molecularly targeted imaging was accomplished with intravenous injection of BR55 clinical-grade microbubbles (Bracco Suisse, Geneva, Switzerland) that bind to human and murine VEGFR2 (29,30) (see Appendix E1 [online]). To allow for comparison of tumors of different sizes, a subset of PDAC mice (18 mice and 28 tumors) were imaged with VEGFR2-targeted microbubbles 1–2 weeks after hypoechoic foci were first identified with 40-MHz B-mode imaging to allow interval growth to a larger diameter. To determine the binding specificity of VEGFR2-targeted microbubbles, the molecularly targeted US signal from VEGFR2-targeted microbubbles and nontargeted control microbubbles (Bracco Suisse) was compared in a subset of PDAC mice (seven mice and 10 tumors). Each mouse received two separate, sequential injections of VEG-FR2-targeted microbubbles and nontargeted control microbubbles in random order. After the first injection of microbubbles, the molecularly targeted US sequence was performed (see Appendix E1 [online]) and was followed by a waiting period of 30 minutes to allow microbubbles to clear from the blood pool (31–34). Then, the second injection of microbubbles was administered, and the US sequence was performed by using the aforementioned protocol. This procedure was performed with the US transducer fixed in place to be able to acquire the signal intensities in the same field of view with both microbubble types.

US Image Analysis

Motion-compensated data analysis on stored cine loops of perfusion and targeted imaging was performed by using commercially available analysis software (VevoCQ; VisualSonics) and is described in Appendix E1 (online). Briefly, a region of interest (ROI) was manually drawn around tumors or normal pancreas tissue, and molecular-targeted imaging signals were analyzed in random order by one reader (S.B.M., with 2 years of experience). Targeted imaging signals (in linear arbitrary units [lau]) in the ROIs were then calculated with the destruction-replenishment method (see Appendix E1 [online]) (31–34). Colorimetric maps of peak enhancement perfusion profiles were analyzed for patterns of peripheral or uniform distribution of functional vascularity (see Appendix E1 [online]) (35).

Ex Vivo Analysis of Pancreas Tissue

After scanning, the mice were euthanized, and pancreata were excised after in vivo tissue fixation (see Appendix E1 [online]) to minimize automatic self-digestion of the pancreas. Pancreas and spleen (for landmark reference) tissues were fixed and prepared as 8-μm frozen sections on microscope slides for hematoxylin-eosin staining (M.A.P., by following standard protocols [36]) and immunofluorescence staining for VEG-FR2 and CD31 (S.B.M., by following standard protocols to validate VEGFR2 expression on tumor neovasculature and for quantitative assessment of VEGFR2 expression; see Appendix E1 [online]).

Slides of hematoxylin-eosin–stained and scanned (×20 magnification, Nano-zoomer, Hamamatsu, Japan) samples were analyzed for the presence of foci of pancreatic cancer by a blinded pathologist (E.S.S., with 8 years of experience). Analysis of VEGFR2 and CD31 colocalization and quantitative VEGFR2 immunofluorescence signal was performed by S.B.M. (with 8 years of experience; see Appendix E1 [online]).

Statistical Analysis

Statistical analyses (Wilcoxon rank sum tests, linear mixed-effects model, and 95% confidence intervals) are detailed in the Appendix E1 (online). A *P* value of less than .05 was considered to indicate a significant difference. Stata software release 13.1 (StataCorp, College Station, Tex) was used for the statistical analyses.

Results

In Vivo US of PDAC and Normal Pancreas

VEGFR2-targeted US signal was quantified in 90 tumors formed within the pancreata of 44 PDAC mice (mean age, 6.2 weeks ± 1.2; range, 3.3–8.9 weeks) and compared with VEGFR2-targeted US signal in 64 pancreata of WT mice (mean age, 5.4 weeks ± 1.3; range, 3.6–8.3 weeks of age) (Fig 2). The 90 tumors (mean diameter, 2.6 mm ± 1.5; range, 0.7–7.4 mm) were identified across the entire pancreas, with 15 tumors (mean diameter, 3.8 mm ± 1.6; range, 1.7–7.4 mm) in the head of the pancreas and 75 tumors (mean diameter, 2.4 mm ± 1.3; range, 0.7–6.6 mm) throughout the body and/or tail of the pancreas.

Overall for all tumor sizes, VEG-FR2-targeted US signal intensity was significantly higher (26.8-fold; $P < .001$) in PDAC (mean intensity, 6.7 lau ± 8.5; range, 0–57.4 lau; Fig 2b)

when compared with VEGFR2-targeted signal intensity in normal, control pancreata of WT mice (mean intensity, 0.25 lau ± 0.25; range, 0.0–1.2 lau; Table).

The VEGFR2-targeted US signal distribution among PDAC lesions was further analyzed by location (tail and/ or body vs head). Signal intensities obtained from PDAC in the tail and/ or body (n = 75 tumors) were significantly higher (mean intensity, 6.8 lau ± 8.8; range, 0–57.4 lau; P < .001) than those in normal pancreas in WT mice but were not significantly different compared with signal intensities (mean intensity, 6.5 lau ± 6.8; range, 0–23 lau; P = .97) in PDAC located in the pancreatic head (n = 15).

The distribution of VEGFR2-targeted US signal intensity in PDAC was further analyzed on the basis of tumor size (Fig 2). Notably, smaller tumors less than 3 mm in diameter (n = 62 tumors; mean diameter, 1.8 mm ± 0.6; range, 0.7–3.0 mm) had a significantly higher (P = .024) VEGFR2-targeted US signal intensity (1.7-fold higher; mean intensity, 7.7 lau ± 9.3; range, 0.2–57.4 lau) compared with tumors larger than 3 mm in diameter (n = 28; mean diameter, 4.4 mm ± 1.2 [range, 3.01–7.4 mm]; mean intensity, 4.6 lau ± 5.8 [range, 0–23.0 lau]; Table). Overall, there was a trend (P = .098) for the targeted US molecular imaging signal to decrease with tumor diameter.

In a subset of mice, control non-targeted microbubbles were injected during the same imaging session as the VEGFR2-targeted microbubbles to validate binding specificity of the VEG-FR2-targeted microbubbles. VEGFR2-targeted US signal was significantly higher (Fig 3; mean intensity, 8.3 lau ± 7.1; range, 1.7–26.2 lau; P < .001) compared with nontargeted control microbubble experiments (mean intensity, 2.6 lau ± 2.7; range, 0.1–7.4 lau).

To determine if the in vivo VEGFR2-targeted US signal differences observed between small (<3 mm) and large (>3 mm) PDAC may have been due to a change in functional vasculature, perfusion analysis was performed. In small pancreatic tumors (<3 mm), 10% (four of 38) demonstrated a dominant peripheral perfusion pattern, while most (90%; 34 of 38) showed a uniform perfusion pattern (Fig 4). In larger PDAC (>3 mm), the perfusion patterns were different; 42% of tumors (eight of 19) showed a dominant peripheral perfusion pattern, with the remaining tumors showing a uniform perfusion pattern. These perfusion patterns were in good agreement with the distribution patterns of VEGFR2-targeted US signal patterns on US molecular images (peripheral or uniform; κ = 0.86; 95% confidence interval: 0.67, 1.00; Fig 4 and Table).

Ex Vivo Analysis of Pancreatic Tissue

PDACs developing in transgenic mice were characterized as having a dense stroma, similar to that described in human PDAC (Figs 3, 4). Ex vivo immunostaining of tumor vessels demonstrated that VEGFR2 expression levels were significantly higher (P < .001) in PDAC (mean fluorescent intensity, 499.4 arbitrary units [au] ± 179.1) compared with normal, WT pancreas tissues (mean fluorescent intensity, 232.9 au ± 83.7). In normal, WT pancreas, low-level VEGFR2 expression was observed in blood vessels associated with normal acinar cells. VEGFR2 was expressed in small capillaries of the pancreatic islets (37). There was no significant difference between the size of the tumor and the expression levels of VEGFR2 in the vasculature (P = .81).

Discussion

In this study, an imaging strategy for earlier PDAC detection with US and a clinical-grade VEGFR2-targeted microbubble contrast agent was tested in a transgenic mouse model. Overall, PDAC was visualized with 26.8-fold higher mean VEGFR2-targeted US signal intensity compared with normal WT pancreas. In particular, small (<3-mm) tumors showed highest VEG-FR2-specific US signals. Thus, US with microbubble contrast agents targeted to angiogenesis markers, such as VEG-FR2, expressed early in pancreatic carcinogenesis may be further developed as a promising new strategy for earlier PDAC detection.

Our approach for developing an imaging strategy to identify small PDAC lesions leveraged one of the hallmarks of cancer, the recruitment of new blood vessels (neoangiogenesis). When small tumors grow beyond 0.2–2 mm in diameter (10^5 to 10^6 cells), the surrounding vasculature is not sufficient to maintain the metabolic need for oxygen and nutrients (22). This stimulates the release of proangiogenic signals from the tumor cells (the angiogenic switch), which triggers the activation of nearby endothelial cells, resulting in continual sprouting of new vessels to help sustain the growing lesion (20,38). In this study, we took advantage of the expression of VEGFR2, present in the neovasculature of many solid cancers, including PDAC (39). The VEGFR2-targeted contrast agent we used has just entered first clinical trials in Europe and the United States (*clinicaltrials.gov* nos. NCT01253213 and NCT02142608) and remains confined to the vasculature because of its size (mean diameter of 1.5 μm) (30,40). This property makes it particularly well suited to visualize molecular markers, such as VEGFR2, expressed on the luminal site of neovascular endothelial cells. The contrast agent specifically helps identify both human and murine VEGFR2 by using a heterodimeric peptide that was directly incorporated into the phospholipid-based microbubble shell, allowing testing of the contrast agent in mouse models (40).

To test our imaging approach, we used a transgenic mouse model with spontaneous PDAC development and phenotypes, such as dense desmoplastic stromal reactions typically seen in human PDAC (41,42). This model develops tumors with features similar to human PDAC, including variable grades of precursor lesions, ductal and anaplastic morphologies, well to moderately differentiated adenocarcinoma, and desmoplastic reactions. Our data suggest that VEGFR2-targeted US signal is significantly increased in PDAC compared with normal pancreatic tissue. In particular, the smallest tumors showed on average the highest mean imaging signals when compared with normal pancreas.

In contrast, when tumors further increased in diameter (beyond 3 mm), mean VEGFR2-targeted US signal decreased when compared with very small tumor foci (<3 mm). Interestingly, while VEGFR2-targeted US signal decreased, there was no significant difference in the expression levels of VEGFR2 in tumors of different sizes, as assessed with immunostaining. This decrease of targeted imaging signal in our study may be explained by reduced vascular perfusion in larger tumors, due to a reduction in the number of functionally intact vessels, thereby decreasing the number of targeted microbubbles that reached their molecular target. It has been shown that the functional tumor vasculature is profoundly diminished in PDAC mouse models, similar to human PDAC, where up to 75% of the

vasculature was determined to be nonfunctional (43,44). This finding is consistent with the tumor perfusion observations with US in our study that showed a change from a homogeneous perfusion pattern in small tumors to a heterogeneous or peripherally dominant perfusion pattern as tumors increased in size. This reduction of functional tumor vasculature had recently been shown to be caused by abnormally high interstitial fluid pressures (fivefold higher) in PDAC compared with low-level pressure in normal mouse pancreas (43). This high pressure in cancer may lead to the collapse of functional vasculature with reduced perfusion (43) and, possibly, the general hypovascular appearance of PDAC at routinely performed contrast-enhanced computed tomography and MR imaging examinations. These considerations underscore the premise that US with molecularly targeted contrast agents may be particularly well suited for detection of PDAC at very small sizes, when the tumor vasculature is still functionally intact and expression of molecular markers such as VEGFR2 can be visualized. Detecting PDAC at such an early, still resectable stage before the onset of micrometastases and perineural invasion is highly desirable and could have a major effect on patient survival if successfully translated into the clinic (45).

We acknowledge the following limitations of our study. The transgenic mouse model we used has a relatively rapid tumor progression with observable tumors within 4–7 weeks of age, which may not relate to the temporal pattern of angiogenesis or VEGFR2 expression in humans or other mouse models of PDAC. Also, the transgenic mice harbor genetic alterations throughout the entire pancreas, with mice developing multifocal lesions of different sizes over time, which is different than in humans, where there may be only one focus of tumor development in an otherwise normal pancreas. Another limitation includes the fact that the perfusion statistics, which influence the contrast agent signaling in mice, may differ in human disease. Clinical studies are warranted to assess diagnostic accuracy of this imaging approach in human PDAC and in benign entities, including benign pancreatic tumors and chronic pancreatitis. Last, our study focused on the use of US with VEGFR2-targeted microbubble contrast agents, and the use of microbubbles targeted to other endothelial markers (eg, endoglin [27], $\alpha v\beta 3$ [27], or Thy1 [46]) may offer different results and/or opportunities in early detection of PDAC.

In conclusion, our study suggests that VEGFR2-targeted US allows detection of small foci of PDAC that spontaneously developed in a transgenic mouse model. Since US is advantageous (readily available and relatively inexpensive, with no exposure to ionizing radiation) for use as a screening modality, the addition of molecular imaging with microbubble contrast agent targeted to angiogenic markers, such as VEGFR2, has great potential for improving earlier detection of PDAC. This study provides a foundation for the development and clinical translation of a molecularly-targeted US-based approach for PDAC detection in high-risk patients.

Supplementary Material

Refer to Web version on PubMed Central for supplementary material.

Acknowledgments

J.K.W. supported by the National Pancreas Foundation, Canary Foundation, Howard S. Stern Research Grant from the Society of Gastrointestinal Radiologists, RSNA, and National Institutes of Health (NIH) grant nos. R21 CA139279 and R01 CA155289-01A1; M.A.P. supported by NIH grant no. R25 CA11868.

We acknowledge the following support at Stanford University: Stanford Neuroscience Microscopy Service, supported by National Institutes of Health grant no. NS069375; Timothy Doyle, PhD, in the Small Animal Imaging Facility; and Philip Beachy, PhD, in the Developmental Biology Program at Stanford University.

Abbreviations

lau	linear arbitrary units
PDAC	pancreatic ductal adenocarcinoma
ROI	region of interest
VEGFR2	vascular endothelial growth factor receptor type 2
WT	wild type

References

1. American Cancer Society. [Accessed September 25, 2014] Cancer Facts and Figures. 2012. http://www.cancer.org/acs/groups/content/@epidemiologysurveilance/documents/document/acspc-031941.pdf
2. Xu Q, Zhang TP, Zhao YP. Advances in early diagnosis and therapy of pancreatic cancer. Hepatobiliary Pancreat Dis Int. 2011; 10(2):128–135. [PubMed: 21459718]
3. Majumder S, Chubineh S, Birk J. Pancreatic cancer: an endoscopic perspective. Expert Rev Gastroenterol Hepatol. 2012; 6(1):95–103. quiz 104. [PubMed: 22149585]
4. Pannala R, Basu A, Petersen GM, Chari ST. New-onset diabetes: a potential clue to the early diagnosis of pancreatic cancer. Lancet Oncol. 2009; 10(1):88–95. [PubMed: 19111249]
5. Pelaez-Luna M, Takahashi N, Fletcher JG, Chari ST. Resectability of presymptomatic pancreatic cancer and its relationship to onset of diabetes: a retrospective review of CT scans and fasting glucose values prior to diagnosis. Am J Gastroenterol. 2007; 102(10):2157–2163. [PubMed: 17897335]
6. Brand RE, Lerch MM, Rubinstein WS, et al. Advances in counselling and surveillance of patients at risk for pancreatic cancer. Gut. 2007; 56(10):1460–1469. [PubMed: 17872573]
7. Ludwig E, Olson SH, Bayuga S, et al. Feasibility and yield of screening in relatives from familial pancreatic cancer families. Am J Gastroenterol. 2011; 106(5):946–954. [PubMed: 21468009]
8. Brentnall TA. Pancreatic cancer surveillance: learning as we go. Am J Gastroenterol. 2011; 106(5): 955–956. [PubMed: 21540900]
9. Shrikhande SV, Barreto SG, Goel M, Arya S. Multimodality imaging of pancreatic ductal adenocarcinoma: a review of the literature. HPB (Oxford). 2012; 14(10):658–668. [PubMed: 22954001]
10. Langer P, Kann PH, Fendrich V, et al. Five years of prospective screening of high-risk individuals from families with familial pancreatic cancer. Gut. 2009; 58(10):1410–1418. [PubMed: 19470496]
11. Adamek HE, Albert J, Breer H, Weitz M, Schilling D, Riemann JF. Pancreatic cancer detection with magnetic resonance cholangiopancreatography and endoscopic retrograde cholangiopancreatography: a prospective controlled study. Lancet. 2000; 356(9225):190–193. [PubMed: 10963196]
12. Topazian M, Enders F, Kimmey M, et al. Interobserver agreement for EUS findings in familial pancreatic-cancer kindreds. Gastrointest Endosc. 2007; 66(1):62–67. [PubMed: 17382940]

13. Kitano M, Kudo M, Yamao K, et al. Characterization of small solid tumors in the pancreas: the value of contrast-enhanced harmonic endoscopic ultrasonography. Am J Gastroenterol. 2012; 107(2):303–310. [PubMed: 22008892]
14. Kitano M, Kudo M, Sakamoto H, Komaki T. Endoscopic ultrasonography and contrast-enhanced endoscopic ultrasonography. Pancreatology. 2011; 11(Suppl 2):28–33. [PubMed: 21464584]
15. Sakamoto H, Kitano M, Suetomi Y, Maekawa K, Takeyama Y, Kudo M. Utility of contrast-enhanced endoscopic ultrasonography for diagnosis of small pancreatic carcinomas. Ultrasound Med Biol. 2008; 34(4):525–532. [PubMed: 18045768]
16. Kersting S, Konopke R, Kersting F, et al. Quantitative perfusion analysis of transabdominal contrast-enhanced ultrasonography of pancreatic masses and carcinomas. Gastroenterology. 2009; 137(6):1903–1911. [PubMed: 19715694]
17. Kersting S, Roth J, Bunk A. Transabdominal contrast-enhanced ultrasonography of pancreatic cancer. Pancreatology. 2011; 11(Suppl 2):20–27. [PubMed: 21464583]
18. Kitano M, Kudo M, Maekawa K, et al. Dynamic imaging of pancreatic diseases by contrast enhanced coded phase inversion harmonic ultrasonography. Gut. 2004; 53(6):854–859. [PubMed: 15138213]
19. Bergers G, Benjamin LE. Tumorigenesis and the angiogenic switch. Nat Rev Cancer. 2003; 3(6): 401–410. [PubMed: 12778130]
20. Hanahan D, Weinberg RA. Hallmarks of cancer: the next generation. Cell. 2011; 144(5):646–674. [PubMed: 21376230]
21. Roskoski R Jr. Vascular endothelial growth factor (VEGF) signaling in tumor progression. Crit Rev Oncol Hematol. 2007; 62(3):179–213. [PubMed: 17324579]
22. Folkman J. Angiogenesis. Annu Rev Med. 2006; 57:1–18. [PubMed: 16409133]
23. Itakura J, Ishiwata T, Shen B, Kornmann M, Korc M. Concomitant over-expression of vascular endothelial growth factor and its receptors in pancreatic cancer. Int J Cancer. 2000; 85(1):27–34. [PubMed: 10585578]
24. Seo Y, Baba H, Fukuda T, Takashima M, Sugimachi K. High expression of vascular endothelial growth factor is associated with liver metastasis and a poor prognosis for patients with ductal pancreatic adenocarcinoma. Cancer. 2000; 88(10):2239–2245. [PubMed: 10820344]
25. Niedergethmann M, Hildenbrand R, Wostbrock B, et al. High expression of vascular endothelial growth factor predicts early recurrence and poor prognosis after curative resection for ductal adenocarcinoma of the pancreas. Pancreas. 2002; 25(2):122–129. [PubMed: 12142733]
26. von Marschall Z, Cramer T, Höcker M, et al. De novo expression of vascular endothelial growth factor in human pancreatic cancer: evidence for an autocrine mitogenic loop. Gastroenterology. 2000; 119(5):1358–1372. [PubMed: 11054395]
27. Deshpande N, Ren Y, Foygel K, Rosenberg J, Willmann JK. Tumor angiogenic marker expression levels during tumor growth: longitudinal assessment with molecularly targeted microbubbles and US imaging. Radiology. 2011; 258(3):804–811. [PubMed: 21339349]
28. Aguirre AJ, Bardeesy N, Sinha M, et al. Activated Kras and Ink4a/Arf deficiency cooperate to produce metastatic pancreatic ductal adenocarcinoma. Genes Dev. 2003; 17(24):3112–3126. [PubMed: 14681207]
29. Pillai R, Marinelli ER, Fan H, et al. A phospholipid-PEG2000 conjugate of a vascular endothelial growth factor receptor 2 (VEGFR2)-targeting heterodimer peptide for contrast-enhanced ultrasound imaging of angiogenesis. Bioconjug Chem. 2010; 21(3):556–562. [PubMed: 20170116]
30. Pysz MA, Foygel K, Rosenberg J, Gambhir SS, Schneider M, Willmann JK. Antiangiogenic cancer therapy: monitoring with molecular US and a clinically translatable contrast agent (BR55). Radiology. 2010; 256(2):519–527. [PubMed: 20515975]
31. Ellegala DB, Leong-Poi H, Carpenter JE, et al. Imaging tumor angiogenesis with contrast ultrasound and microbubbles targeted to alpha(v)beta3. Circulation. 2003; 108(3):336–341. [PubMed: 12835208]
32. Lindner JR, Song J, Xu F, et al. Noninvasive ultrasound imaging of inflammation using microbubbles targeted to activated leukocytes. Circulation. 2000; 102(22):2745–2750. [PubMed: 11094042]

33. Pysz MA, Willmann JK. Targeted contrast-enhanced ultrasound: an emerging technology in abdominal and pelvic imaging. Gastroenterology. 2011; 140(3):785–790. [PubMed: 21255573]
34. Willmann JK, Paulmurugan R, Chen K, et al. US imaging of tumor angiogenesis with microbubbles targeted to vascular endothelial growth factor receptor type 2 in mice. Radiology. 2008; 246(2):508–518. [PubMed: 18180339]
35. Rissanen TT, Korpisalo P, Karvinen H, et al. High-resolution ultrasound perfusion imaging of therapeutic angiogenesis. JACC Cardiovasc Imaging. 2008; 1(1):83–91. [PubMed: 19356410]
36. Deshpande N, Lutz AM, Ren Y, et al. Quantification and monitoring of inflammation in murine inflammatory bowel disease with targeted contrast-enhanced US. Radiology. 2012; 262(1):172–180. [PubMed: 22056689]
37. Brissova M, Shostak A, Shiota M, et al. Pancreatic islet production of vascular endothelial growth factor–a is essential for islet vascularization, revascularization, and function. Diabetes. 2006; 55(11):2974–2985. [PubMed: 17065333]
38. Weis SM, Cheresh DA. Tumor angiogenesis: molecular pathways and therapeutic targets. Nat Med. 2011; 17(11):1359–1370. [PubMed: 22064426]
39. Korc M. Pathways for aberrant angiogenesis in pancreatic cancer. Mol Cancer. 2003; 2(1):8. [PubMed: 12556241]
40. Pochon S, Tardy I, Bussat P, et al. BR55: a lipopeptide-based VEGFR2-targeted ultrasound contrast agent for molecular imaging of angiogenesis. Invest Radiol. 2010; 45(2):89–95. [PubMed: 20027118]
41. Mohammed A, Janakiram NB, Lightfoot S, Gali H, Vibhudutta A, Rao CV. Early detection and prevention of pancreatic cancer: use of genetically engineered mouse models and advanced imaging technologies. Curr Med Chem. 2012; 19(22):3701–3713. [PubMed: 22680929]
42. Olive KP, Tuveson DA. The use of targeted mouse models for preclinical testing of novel cancer therapeutics. Clin Cancer Res. 2006; 12(18):5277–5287. [PubMed: 17000660]
43. Provenzano PP, Cuevas C, Chang AE, Goel VK, Von Hoff DD, Hingorani SR. Enzymatic targeting of the stroma ablates physical barriers to treatment of pancreatic ductal adenocarcinoma. Cancer Cell. 2012; 21(3):418–429. [PubMed: 22439937]
44. Olive KP, Jacobetz MA, Davidson CJ, et al. Inhibition of Hedgehog signaling enhances delivery of chemotherapy in a mouse model of pancreatic cancer. Science. 2009; 324(5933):1457–1461. [PubMed: 19460966]
45. Chan A, Diamandis EP, Blasutig IM. Strategies for discovering novel pancreatic cancer biomarkers. J Proteomics. 2013; 81(0):126–134. [PubMed: 23026552]
46. Foygel K, Wang H, Machtaler S, et al. Detection of pancreatic ductal adenocarcinoma in mice by ultrasound imaging of thymocyte differentiation antigen 1. Gastroenterology. 2013; 145(4):885–894. e3. [PubMed: 23791701]
47. Rognin, NG.; Campos, R.; Thiran, JP., et al. A new approach for automatic motion compensation for improved estimation of perfusion quantification parameters in ultrasound imaging. Presented at the 8é Congrès Français d'Acoustique; Tours, France. 2006.

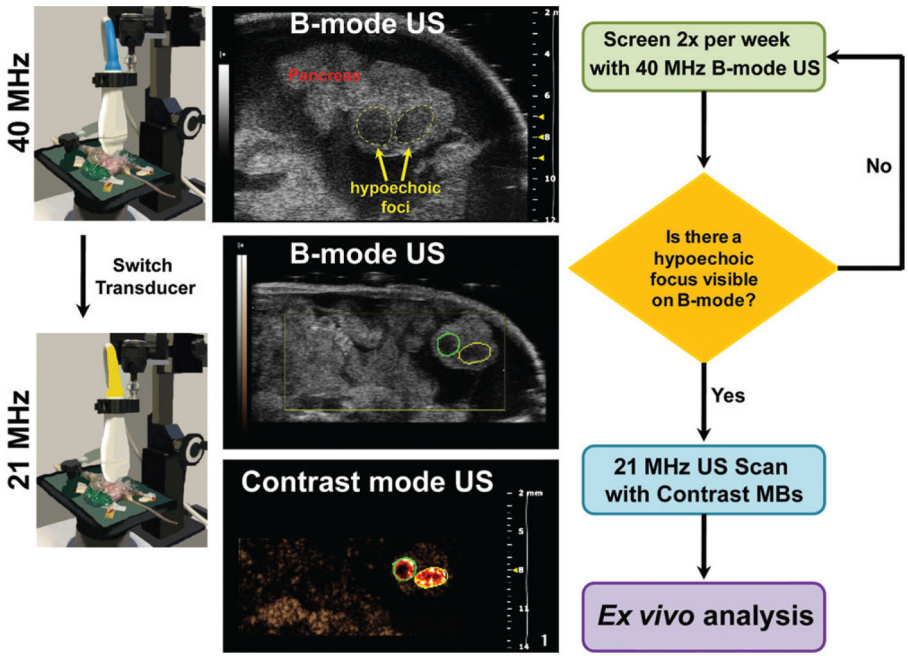

Figure 1.

The experimental design for imaging small foci of PDAC in transgenic mice is demonstrated. Transgenic mice were first scanned with high-resolution B-mode anatomic US (40-MHz transducer), starting at 3 weeks of age, and continuing twice per week until subtle hypoechoic or heterogeneous foci were seen. The same region was then scrutinized with US by using VEGFR2-targeted (or nontargeted) microbubbles *(MBs)* by using a 21-MHz transducer. After imaging, the mouse was sacrificed, and tissues (pancreas and spleen as anatomic reference structures) were collected for ex vivo histologic examination and immunostaining.

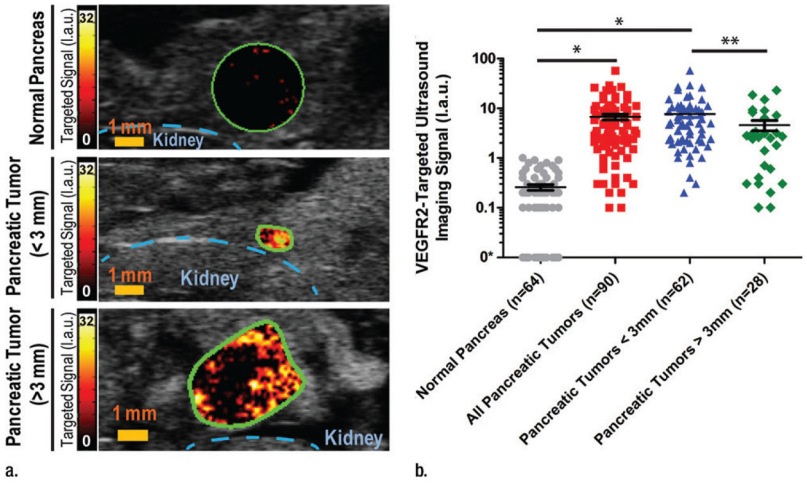

Figure 2.

Demonstration of VEGFR2-targeted US signal observed in small foci of PDAC. **(a)** Representative VEGFR2-targeted US signal (green ROIs) is shown in normal pancreas (top panel) and two foci of PDAC in two different transgenic mice (middle and lower panels). Representative examples of a very small tumor (1.2 mm, middle panel) and a larger tumor (3.1 mm, bottom panel) are shown. The colorimetric maps of VEGFR2-targeted US signal intensities are overlaid onto the anatomic B-mode images. The outline of the kidney is shown in blue. Scale bar = 1 mm. **(b)** Dot plot summarizes mean VEGFR2-targeted US signal (in linear arbitrary units) measured in normal pancreas (n = 64; gray circles) and all pancreatic tumors (n = 90; red squares). Pancreatic tumors were further analyzed by tumor diameter—smaller than 3 mm (n = 62, blue triangles) and larger than 3 mm (n = 28, green diamonds). Note that the VEGFR2-targeted US signal is plotted on a log-10 scale to allow all the data in range to be visualized. * = P < .001, ** = P < .024.

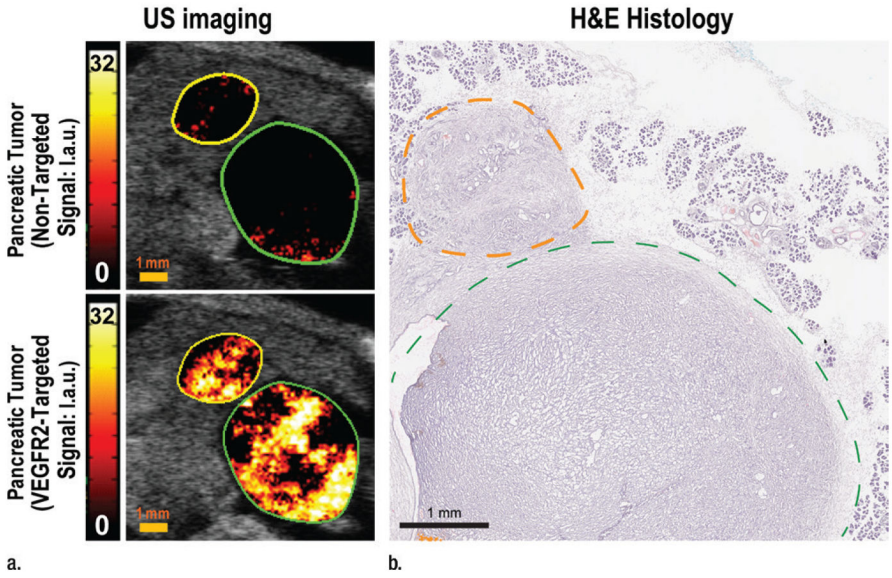

Figure 3.

Images demonstrate validation of binding specificity of targeted microbubbles to VEGFR2 in PDAC tumors in an intra-animal comparison experiment. **(a)** Representative transverse targeted US images of the body and/or tail of the pancreas show two adjacent foci of PDAC (small tumor outlined with yellow ROI; larger tumor outlined in green ROI), imaged sequentially with nontargeted microbubbles (top panel) and VEGFR2-targeted microbubbles (bottom panel). Note the high targeted imaging signal intensity with VEGFR2-targeted contrast agent and the low imaging signal intensity with the nontargeted contrast agent. **(b)** Corresponding hematoxylin-eosin *(H&E)*–stained sample (original magnification, ×20) confirms the presence of two adjacent foci of PDAC. Scale bar = 1 mm.

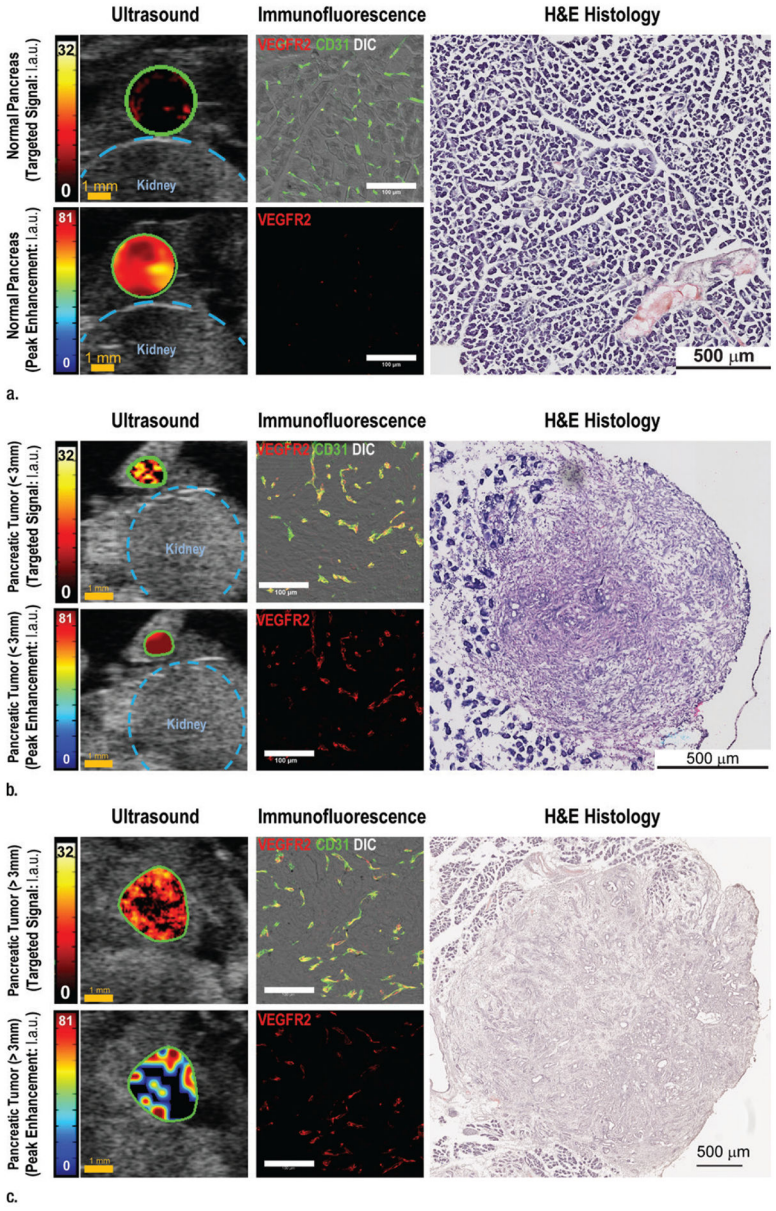

Figure 4.

Images demonstrate in vivo VEGFR2-targeted US signal (top left panel), tumor perfusion (bottom left panel), and ex vivo VEGFR2 expression (panels in the middle column) in **(a)** a normal pancreas, **(b)** a small PDAC (<3 mm group), and **(c)** a larger PDAC (>3 mm group). VEGFR2-targeted US signal intensities (green ROIs) are overlaid on anatomic B-mode images; the kidney is outlined in blue; scale bar = 1 mm. Corresponding perfusion images show different enhancement patterns in small tumors with relatively homogeneous perfusion in the small tumor and heterogeneous, predominantly peripheral enhancement pattern in the larger tumor. Confocal micrographs show VEGFR2 expression (red) and blood vessels (CD31, green) overlaid on the differential interference contrast bright-field image (top image, middle column) or VEGFR2 expression alone (bottom image, middle column). Note

that there is only minimal VEGFR2 expression in normal pancreas. Also note that VEGFR2 expression is similar in small versus large tumors. Scale bar = 100 μm. Right panel shows hematoxylin-eosin *(H&E)*–stained histologic sample of the corresponding pancreatic tissue, confirming the presence of PDAC on **b** and **c** and normal pancreatic tissue on **a**. Scale bar = 500 μm.

Table

Summary of In Vivo VEGFR2-targeted US Signal Intensity and Ex Vivo VEGFR2 Immunofluorescence Intensities in WT and PDAC Mice

Parameter	Normal Pancreas in 64 WT Mice	PDAC Mice (44 mice)		
		All Tumors (90 tumors in all locations in the pancreas)	Tumors Smaller Than 3 mm in Diameter (62 tumors)	Tumors Larger Than 3 mm in Diameter (28 tumors)
Age at time of scan (wk)	5.4 ± 1.3 (3.6–8.3)	6.2 ± 1.2 (3.3–8.9)	6.0 ± 1.3 (3.3–8.9)	6.7 ± 0.8 (4.7–8.8)
Tumor diameter (mm)	NA	2.6 ± 1.5 (0.7–7.4)	1.8 ± 0.6 (0.7–3.0)	4.4 ± 1.2 (3.01–7.2)
VEGFR2-targeted US signal intensity (lau)	0.25 ± 0.25 (0.0–1.2)	6.7 ± 8.5 (0.0–57.4)	7.7 ± 9.3 (0.2–57.4)	4.6 ± 5.8 (0.0–23.0)
Percentage of peripheral perfusion pattern (%)	NA	NA	10 (four of 38)	42 (eight of 19)
Ex vivo VEGFR2 mean fluorescent intensity (au)	232.9 ± 83.7 (132.9–383.2)	499.4 ± 179.1 (197.9–767.7)	486.1 ± 138.7 (286.5–765.5)	526.0 ± 251.0 (197.9–767.7)

Note.—Unless indicated otherwise, data are means ± standard deviations, with ranges in parentheses. Note that tumors of varying size were sometimes visualized within the same mouse. VEGFR2-targeted US signal intensity in normal pancreas compared with all pancreatic tumors yielded a difference of $P < .001$; VEGFR2-targeted US signal intensity in PDAC tumors smaller than 3 mm compared with PDAC tumors larger than 3 mm in diameter yielded a difference of $P = .024$; correlation analysis of VEGFR2-targeted US signal intensity with peripheral perfusion pattern for PDAC tumors smaller than 3 mm and larger than 3 mm in diameter yielded a κ value of 0.86 (95% confidence interval: 0.67, 1.00); ex vivo VEGFR2 immunofluorescence mean fluorescent intensity in normal pancreas compared with all PDAC tumors yielded a difference of $P < .001$; ex vivo VEGFR2 immunofluorescence mean fluorescent intensity in PDAC tumors smaller than 3 mm compared with PDAC tumors larger than 3 mm diameter yielded a difference of $P = .81$. NA = not applicable